# Trapped Conformational States of Semiquinone ($D^{+\bullet}Q_B^{-\bullet}$) Formed by B-Branch Electron Transfer at Low Temperature in *Rhodobacter sphaeroides* Reaction Centers†

M. L. Paddock,* M. Flores,‡ R. Isaacson, C. Chang, E. C. Abresch, P. Selvaduray, and M. Y. Okamura

*Department of Physics, University of California, San Diego, La Jolla, California 92093*

*Received May 1, 2006; Revised Manuscript Received September 15, 2006*

ABSTRACT: The reaction center (RC) from *Rhodobacter sphaeroides* captures light energy by electron transfer between quinones $Q_A$ and $Q_B$, involving a conformational gating step. In this work, conformational states of $D^{+\bullet}Q_B^{-\bullet}$ were trapped (80 K) and studied using EPR spectroscopy in native and mutant RCs that lack $Q_A$ in which $Q_B$ was reduced by the bacteriopheophytin along the B-branch. In mutant RCs frozen in the dark, a light induced EPR signal due to $D^{+\bullet}Q_B^{-\bullet}$ formed in 30% of the sample with low quantum yield (0.2%−20%) and decayed in 6 s. A small signal with similar characteristics was also observed in native RCs. In contrast, the EPR signal due to $D^{+\bullet}Q_B^{-\bullet}$ in mutant RCs illuminated while freezing formed in ∼95% of the sample did not decay ($\tau > 10^7$ s) at 80 K (also observed in the native RC). In all samples, the observed *g*-values were the same ($g = 2.0026$), indicating that all active $Q_B^{-\bullet}$'s were located in a proximal conformation coupled with the nonheme $Fe^{2+}$. We propose that before electron transfer at 80 K, the majority (∼70%) of $Q_B$, structurally located in the distal site, was not stably reducible, whereas the minority (∼30%) of active configurations was in the proximal site. The large difference in the lifetimes of the unrelaxed and relaxed $D^{+\bullet}Q_B^{-\bullet}$ states is attributed to the relaxation of protein residues and internal water molecules that stabilize $D^{+\bullet}Q_B^{-\bullet}$. These results demonstrate energetically significant conformational changes involved in stabilizing the $D^{+\bullet}Q_B^{-\bullet}$ state. The unrelaxed and relaxed states can be considered to be the initial and final states along the reaction coordinate for conformationally gated electron transfer.

Electron transfer reactions play crucial roles in many biological processes such as photosynthesis and respiration. In many cases, the observed rate of electron transfer depends upon the electronic coupling and free energy differences according to the Marcus theory (*1*). In other cases, the observed rate of electron transfer is limited by another process such as conformational gating (*2*). Examples include protein motion ($bc_1$ complex), proton transfer, solvation changes, or ligand binding steps that convert an inactive configuration of a protein to a state active in electron transfer (*3*). The electron transfer reaction $Q_A^{-\bullet}Q_B \rightarrow Q_AQ_B^{-\bullet}$ between the quinone electron acceptors $Q_A$ and $Q_B$ in the bacterial reaction center (RC[1]) from *Rhodobacter (Rb.) sphaeroides* is an example of a gated electron transfer process. The reaction rate was shown to depend upon protein conformation based on changes of electron transfer upon freezing to cryogenic temperatures (*4*, *5*), cross-linking of the protein subunits (*6*), and embedding the protein in a glassy matrix (*7*) or PVA film (*8*). Furthermore, quinone ($Q_A$) substitution studies showed that the observed rate of electron transfer was independent of the driving force, indicating a conformational gating mechanism (*9*). In this work, we investigate the properties of different conformational states of the RC trapped by freezing the protein at cryogenic temperatures. High energy states of $D^{+\bullet}Q_B^{-\bullet}$ were formed in a mutant RC (previously described in ref 10 (*10*)) in which electron transfer to $Q_B$ occurred *via* the low potential electron donor, bacteriopheophytin, by enhancing electron transfer along the B-branch of the RC (*11*, *12*). This allowed the high energy state to be trapped at low temperature and the kinetic and spectroscopic properties to be measured.

The RC of the purple non-sulfur bacterium *Rb. sphaeroides* is the pigment protein complex responsible for the initial light induced electron transfer reactions that convert light energy into chemical energy (*13*, *14*). The cofactors in the RC are arranged in two parallel branches (designated A-branch and B-branch) across the protein (Figure 1). Electron transfer normally occurs almost exclusively through the A-branch from the primary donor, a bacteriochlorophyll dimer D, through monomeric bacteriochlorophyll ($B_A$), bacteriopheophytin ($H_A$) to ubiquinone ($Q_A$) in about 200 ps followed by gated electron transfer to $Q_B$, the secondary quinone electron acceptor. The oxidized donor $D^+$ is reduced by a cytochrome $c_2$ molecule. Proton coupled electron transfer through the A-branch to $Q_B$ utilizes two photons, two photoelectrons, and two protons to form a quinol molecule $Q_BH_2$ within the pigment−protein RC complex (eq 1) (*18*−

† This work was supported by National Institutes of Health Grant GM 41637.

* Corresponding author. Phone: (858) 534-2504. Fax: (858) 822-0007. E-mail: mpaddock@physics.ucsd.edu.

‡ Current affiliation: Max-Planck Institut für Bioanorganisch Chemie, Stiftstrasse 34-36, D-45470 Mühlheim an der Ruhr, Germany.

[1] Abbreviations: RC, reaction center; D, primary donor, dimer of bacteriochlorophylls; $Q_A$, primary quinone electron acceptor; $Q_B$, secondary quinone electron acceptor; $k_{AB}^{(1)}$, rate of first electron transfer from $Q_A^{-\bullet}$ to $Q_B$.

10.1021/bi060854h CCC: $33.50 
Published on Web 11/02/2006

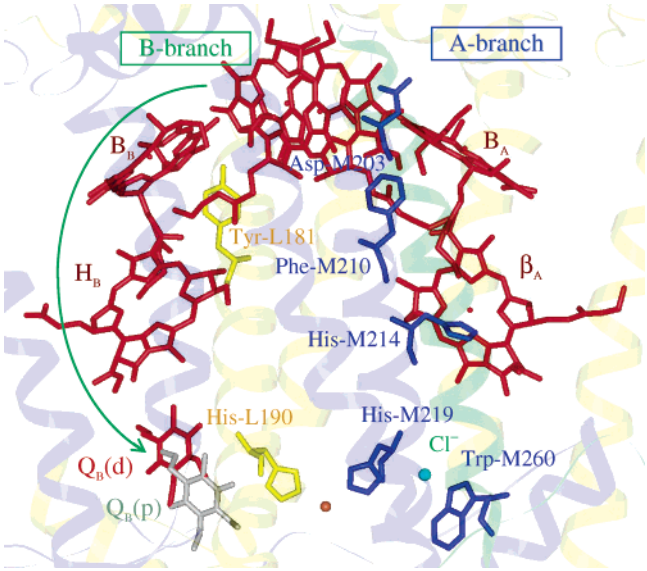


FIGURE 1: Structure of the RC cofactors in the B-branch mutant used in this study (*10*) (pdb ID code 1YF6). Shown are the cofactors in red, imbedded in the backbone structure of the RC, in light yellow (L subunit), blue (M subunit), and green (H subunit). Shown also are the $Fe^{2+}$ ligands, His-M219 (blue) and His-L190 (yellow), and the five mutation sites: (1) Trp-M260 (*15*) and the consequential binding of a $Cl^-$ anion and the displacement of the primary quinone electron acceptor, $Q_A$ (*16*); (2) His-M214 results in the inclusion of a $Mg^{2+}$ in the porphoryn ring creating $\beta_A$ (*17*); (3) Phe-M210; (4) Asp-M203; and (5) Tyr-L181 along the B-branch. These RCs have only one functionally active quinone electron acceptor located at the $Q_B$ site. $Q_B$ is bound at the distal (d) location and is, hence, labeled $Q_B(d)$. For reference, we show the location of $Q_B^{-\bullet}$ in the native RC superimposed on the mutant structure in green-gray; this quinone is located at the proximal (p) location and is labeled $Q_B(p)$. $H_A$ and $H_B$ are bacteriopheophytins, $B_A$ and $B_B$ are bacteriochlorophylls, and the subscript A or B refers to the cofactor binding to the A-branch or B-branch, respectively.

*20*) as follows:

$$Q_B + 2h\nu + 2e^- + 2H^+ \rightarrow Q_BH_2 \qquad (1)$$

where $Q_BH_2$ is the resultant quinol. The protons for this reaction are acquired from the cytoplasm. Following formation, the quinol can diffuse within the membrane to the cyt $bc_1$ complex, where it is oxidized, and the protons are transferred to the periplasm. The electrons are shuttled between the cyt $bc_1$ complex and the RC by a mobile cyt $c_2$ electron carrier (*14*).

The reduction process of $Q_B$ occurs in two sequential photoinduced electron transfer steps that result in electron transfer from a primary electron donor $Q_A^{-\bullet}$ to $Q_B$. The first electron transfer step, which is the focus of this work, occurs with an observed rate constant $k_{AB}^{(1)}$, which is in the range $10^4-10^5\ s^{-1}$ (*9*, *21*, *22*). The kinetic decay is best described by the sum of several exponential components indicating that the reaction involves more than one step (*22*, *23*). The independence of the transfer rate from the driving force for electron transfer (*9*) has led to the proposal that the reaction is conformationally gated (*24*).

An important functional feature of the RC is the position of $Q_B$. The location of quinone in the $Q_B$ pocket is one of the least well determined parts of the RC crystal structure. This is in part due to the function of $Q_B$ as a mobile electron carrier. Early low-resolution crystal structures showed $Q_B$ to be relatively poorly defined (*25*). More recent high-resolution structures show $Q_B$ to be bound in two primary positions, a distal position in which the quinone head group is outside of the binding pocket and has only one H-bond with the protein (*26*, *27*) and a proximal position in which $Q_B$ is bound by 4 H-bonds in the binding pocket (*27*, *28*) (Figure 1). These sites are displaced by ~5 Å. However, the preferred binding position is unclear. In different crystal structures, the fraction of $Q_B$ bound at the two sites varied from nearly all distal (*26*, *27*) to approximately 50% distal (*28*) to nearly all proximal (*29*). Furthermore, the preferred binding position may be a function of the cryoprotectant (if the crystal is frozen) and temperature (*30*). In contrast, $Q_B^{-\bullet}$, the reduced anionic semiquinone, has always been found to be bound in the proximal site (*27*, *28*), consistent with the stabilization of the negative charge by H-bonds. This binding position is supported by EPR, ENDOR (*31*, *32*), and FTIR (*33*, *34*) spectroscopic studies.

The X-ray crystal structure of the mutant RC used in this study, which includes the Ala-M260 → Trp mutation that displaces $Q_A$ (described in more detail below), showed $Q_B$ to be bound predominantly in the distal site (*10*). However, in the crystal structure of a mutant RC with only the single Ala-M260 → Trp mutation, McAuley et al. (*16*) reported that $Q_B$ was bound at the proximal site. Thus, in RCs containing the Ala-M260 → Trp mutation, $Q_B$ has been observed in both the distal (*10*) and proximal (*16*) sites, as has been reported in the native RC.

The detailed interactions with the structure (conformation) of the surrounding protein are major factors in determining the properties of $Q_B$. One well studied structural change is the proton uptake induced by the formation of $Q_B^{-\bullet}$ (*35*, *36*). Located near the $Q_B$ site are a number of acidic residues, including Asp L213, Glu L212, and Asp L210, that change their protonation state upon quinone reduction. The changes in the protonation state of the charged residues have been studied by computational methods (*37*, *38*) and infrared spectroscopy (*39*, *40*). In addition to changes in protonation, the positions of nearby dipolar species will likely change in response to the charge introduced upon reduction. These include the positions of polar residues and bound water molecules around $Q_B$.

The different positions for $Q_B$ observed in X-ray crystal structures led to the idea that the conformational gating step could be the movement of $Q_B$ from the distal to the proximal site, which involves a movement of ~5 Å and a rotation of the head group along the isoprenoid tail. However, this is unlikely, given the independence of the rate on the length of the isoprenoid chain of $Q_B$ (*9*, *41*, *42*) and the observation of the same rate constant $k_{AB}^{(1)}$ measured in a mutant RC in which $Q_B$ was predominantly structurally located in the proximal site (*29*). Another possible gating mechanism involves a conformational change in the protein that is required to favor the $Q_A^{-\bullet}Q_B \rightarrow Q_AQ_B^{-\bullet}$ reaction. In this case, the free energy is initially unfavorable, but becomes favorable because of a change in protein structure. This mechanism is supported by the observations of Li et al. (*23*), which state that the replacement of $Q_A$ with low potential quinones resulted in a fast component of electron transfer that was driving force dependent.

The present study was designed to examine changes in the environment of $Q_B^{-\bullet}$ that result from its reduction. The

configurations of the protein before and after reduction were trapped by freezing RCs to cryogenic temperatures as has been done previously (*4*, *5*). Because $Q_B^{-\bullet}$ cannot be formed by electron transfer from $Q_A^{-\bullet}$ in a significant fraction of samples frozen in the dark in the native RC (*5*, *43*), we developed a modified RC (Figure 1) in which electron transfer to $Q_B$ occurred through the B-branch bacteriopheophytin ($H_B^{-\bullet}$) (*10*, *44*−*47*), which has a much greater driving force for electron transfer (*12*). This allows higher energy states of $Q_B^{-\bullet}$ to become populated (*47*). To obtain significant electron transfer along the B-branch, we constructed a mutant RC that incorporated four mutations designed to increase the efficiency of B-branch electron transfer and a mutation, Ala-M260 → Trp, designed to remove $Q_A$ (*15*, *16*). The mutations are Leu-M214 → His (*48*), Gly-M203 → Asp (*49*−*51*), Tyr-M210 → Phe, and Phe-L181 → Tyr (*48*, *52*, *53*). The construction of this quintuple mutant was previously reported (*10*). In the quintuple mutant, we could form $Q_B^{-\bullet}$ via B-branch electron transfer at room temperature (*54*) and in the frozen state (*47*), which allowed us to form and trap an intermediate state involved in the reduction of $Q_B$.

EPR spectroscopy was used to investigate the properties of the charge separated state $D^{+\bullet}Q_B^{-\bullet}$ in RCs frozen to cryogenic temperature (80 K) either under illumination in which the protein is allowed to relax or frozen in the dark followed by illumination in which the protein is trapped in the initial unrelaxed configuration. The *g*-values of the EPR signals, the dependence of the signal amplitude as a function of the light intensity, and the lifetime of the charge separated states were measured. Because the protein may be present as an ensemble of states with different configurations, EPR measurements in the frozen state can serve to map out the distribution of protein conformational states. The lifetimes for charge recombination ($D^{+\bullet}Q_B^{-\bullet} \rightarrow DQ_B$) were used to assess the differences in the energies of the charge separated states formed by freezing in the dark or in the light, which results in the formation of a stable $D^{+\bullet}Q_B^{-\bullet}$ state (*54*). A preliminary account of this work has been presented previously (*47*).

## MATERIALS AND METHODS

*Construction of the Quintuple B-Branch Mutant RC*. The mutations were incorporated as previously described (*10*) with the following nucleic acid change(s): GCC → TGG (Ala-M260 → Trp), CTG → CAC (Leu-M214 → His), TAC → TTC (Tyr-M210 → Phe), GGT → GAC (Gly-M203 → Asp), TTC → TAC (Phe-L181 → Tyr). The RC proteins were isolated from semi-aerobically grown cells as described (*55*) with an optical ratio OR = $A^{280}/A^{802}$ < 1.3. $Q_B$ was reconstituted by adding an ∼3-fold excess of $UQ_{10}$ in 1% LDAO prior to dialysis against TMK (2 mM Tris-HCl at pH 8, 0.04% $\beta$-D-maltoside, and 5 mM KCl).

*EPR Measurements*. EPR spectroscopy ($d\chi''/dH$ vs H) was performed at a microwave frequency of 9 GHz at $T = 80$ K as previously described (*56*). Two samples were made from the same RC material (∼100$\mu$M RC). It was necessary to incubate the sample in 20−100 $\mu$M ferricyanide/ferrocyanide to oxidize any $Q_B^{-\bullet}$ in the sample prior to illumination; in some untreated samples, as much as 45% $Q_B^{-\bullet}$ was present prior to illumination. Once treated, one sample was frozen in liquid nitrogen in the dark. The other was illuminated by a projector (∼1 W/cm$^2$ of white light, ∼5 s) and frozen in liquid nitrogen under illumination. Upon illumination in the EPR cavity with a similar projector, a charge separated signal was generated in the sample frozen in the dark ($T = 80$ K). The amplitude of this signal was measured as a function of the relative intensity of the actinic white light source. The intensity was decreased by using a series of neutral density filters. Upon turning off the exciting light, charge recombination was observed. The rate was measured by monitoring the time dependence of the signal at a fixed magnetic field value close to $B = 3217$ G. The samples were stored in liquid nitrogen and reassessed ∼1 year ($10^7$ s) later.

*Model for Fit of Signal as a Function of Light Intensity*. Here, we describe the model used to fit the dependence of the signal amplitude on the intensity of the actinic light. The basic equation is

$$DQ_B \underset{k_{BD}}{\overset{k_{ex}}{\rightleftharpoons}} D^{+\bullet}Q_B^{-\bullet} \qquad (2)$$

where $DQ_B$ is the RC in the ground state, $D^{+\bullet}Q_B^{-\bullet}$ is the RC in the excited charge separated state, and $k_{ex}$ and $k_{BD}$ are the excitation and recombination rate constants, respectively. The rate of excitation is determined by the product of the quantum efficiency $\Phi_B$ and the rate of light absorption $k_I$. As the sample is excited with light (starting at time $t = 0$), the $D^{+\bullet}Q_B^{-\bullet}$ state accumulates until the rate of recombination competes with the rate of excitation. When these two rates are equal, a steady-state population is reached (i.e., no further changes in absorbance are observed). The steady-state level of the change in absorption ($\Delta A^{865}{}_{ss}$) is determined by the ratio of the excitation to the sum of the excitation and recombination rate constants as shown in eq 3.

$$\Delta A^{865}{}_{ss} = \Delta A^{865}{}_{max}\frac{k_{ex}}{k_{ex}+k_{BD}} = \Delta A^{865}{}_{max}\frac{\sigma I\Phi_B}{\sigma I\Phi_B + k_{BD}} = \Delta A^{865}{}_{max}\frac{1}{1+I_{1/2}/I} \qquad (3)$$

where $\Delta A^{865}{}_{max}$ is the maximum change in absorption, and the rate of excitation is expressed as the product of the absorption cross section ($\sigma$), light intensity ($I$), and quantum efficiency ($\Phi_B$). This equation describes a curve that increases linearly with increasing $I$ when $\sigma I\Phi_B \ll k_{BD}$ but reaches a saturating value of $\Delta A^{865}{}_{max}$ when $\sigma I\Phi_B \gg k_{BD}$. The value of $I$ at half saturation, $I_{1/2}$, occurs at $k_{BD}/\sigma\Phi_B$. For some samples, it was necessary to fit the data with the sum of two terms, each with its own values of $\Delta A^{865}{}_{max}(i)$ and $I_{1/2}(i)$ (eq 3), where the ($i$) represents the values for the $i$th subpopulation; this is subject to the constraint that the sum of subpopulations is equal to the total, that is, $\Delta A^{865}{}_{max}(\text{total}) = \Sigma_i DA^{865}{}_{max}(i)$.

To estimate the quantum efficiency of the active population, we can compare the ratio of $I_{1/2}$ values assuming that the absorption cross sections are the same (eq 4).

$$\Phi_B/\Phi_A = (k_{BD}/I_{B1/2})(I_{A1/2}/k_{AD}) \qquad (4)$$

where $\Phi_B$ and$\Phi_A$ are the quantum efficiencies for forming $D^{+\bullet}Q_B^{-\bullet}$ and $D^{+\bullet}Q_A^{-\bullet}$, respectively, in the (sub)populations of the sample; $k_{BD}$ and $k_{AD}$ are the recombination rates of the $D^{+\bullet}Q_B^{-\bullet}$ and $D^{+\bullet}Q_A^{-\bullet}$ states, respectively; and $I_{B1/2}$ and

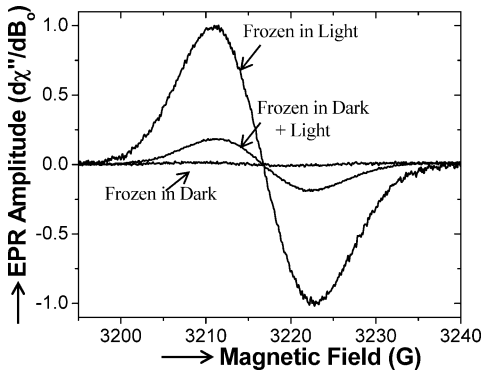


FIGURE 2: EPR spectra ($d\chi''/dH$) in the frozen state ($T = 80$ K) of the B-branch mutant RC samples frozen under illumination (Frozen in Light), frozen in the dark (Frozen in Dark), and illuminated in the dark frozen sample (Frozen Dark + Light). The amplitude of the EPR signal of the dark frozen sample was ~20% of the amplitude of the sample frozen in the light, indicating that a stable charge separation can be formed in a minor fraction of the sample. Note that both traces cross zero at the same value of the magnetic field, showing that the *g*-values are the same in both samples and that the lineshapes (peak-to-trough ratios) are the same. Traces were normalized to the peak amplitude of the signal of the sample frozen under illumination. (Conditions: [RC] ~100 $\mu$M; ID of EPR tube = 0.2 cm; $\nu = 9$ GHz; 80 K; 16 traces were averaged, 30 s per trace.)

$I_{A1/2}$ are the half saturation values for forming the $D^{+\bullet}Q_B^{-\bullet}$ and $D^{+\bullet}Q_A^{-\bullet}$ states, respectively. Because RC samples were made with similar RC concentrations, we expect the assumption that $\sigma$ is the same between samples to introduce at most a systematic uncertainty of ~20%. This is much smaller than the relative differences discussed in this work and, hence, does not affect the conclusions.

## RESULTS

*EPR Signals from Mutant RCs Frozen in the Light and Frozen in the Dark.* EPR spectroscopy was used to monitor the environment and lifetimes of the charge separated states formed in mutant RC samples frozen under illumination and frozen in the dark followed by illumination. In the quintuple mutant sample frozen under illumination, the observed EPR signal had a *g*-value of 2.0026 and a symmetric line shape (see frozen in light trace in Figure 2) that was characteristic of $D^{+\bullet}$ (*57*). The light frozen EPR signal did not decay at 80 K ($\tau > 10^7$s). Upon illumination of the sample in the spectrometer, the signal amplitude was marginally increased (~5%), which is attributed to a minor fraction of RCs in the ground state prior to freezing.

The quintuple mutant RC sample frozen in the dark had essentially no (<1% of maximum) EPR signal (frozen in dark trace, Figure 2) following treatment with ferricyanide to remove any $Q^{-\bullet}$ in the stored sample (see Materials and Methods). However, upon illumination, an EPR signal (frozen in dark + light trace, Figure 2) was generated that decayed (average $\tau = 6$ s) when illumination was terminated. The EPR signals seen in the quintuple mutant (Figure 2) were not observed in samples to which the $Q_B$ binding inhibitor stigmatellin was added, indicating that electron transfer formed the $D^{+\bullet}Q_B^{-\bullet}$ state. The EPR spectra did not indicate the presence of a magnetically uncoupled semiquinone $Q_B^{-\bullet}$, which has an uncoupled *g*-value of 2.0053 (*32*). The uncoupled semiquinone would be expected to result in an observable shift in the *g*-value (2.0036) and introduce an asymmetry in the line shape (1.5:1 ratio in relative amplitude of the peak and trough) (*32*). The absence of the uncoupled semiquinone indicates that the semiquinone spectrum is broadened by its interaction with the high spin $Fe^{2+}$ (*58*).

*Kinetics of Charge Separation and Recombination in Native and Quintuple Mutant RCs.* The kinetics of the formation and decay of the light induced $D^{+\bullet}$ EPR signals were studied by illumination of native and mutant RC samples frozen in the dark ($T = 80$ K) (Figure 3). Following light excitation, the EPR signals in native and quintuple mutant RCs decayed with different kinetics. Following the highest intensity illumination ($I = 0.1$ W/cm$^2$), the majority of the signal in the native RC (Figure 3) decayed with $\tau =$ 30 ms, characteristic of decay from the $Q_A^{-\bullet}$ state ($D^{+\bullet}Q_A^{-\bullet} \rightarrow DQ_A$) (*57*, *59*). A minor component (see arrow in Figure 3) had a significantly slower decay with a $\tau \sim 6$ s. This lifetime was the same as that measured in the quintuple mutant (Figure 3); a slightly better fit was obtained with two exponentials of equal amplitude with time constants $\tau$ of ~2 s and ~10 s, respectively (Figure 4). The same kinetic decay was also observed in all other B-branch mutant RCs (Table 1). The relative fraction of the signal in the native RC that displayed slow kinetics was greater at low light intensity than that at high light intensity (Figure 3) because of the differences in light saturation behavior of the fast and slow components (Figure 5).

The lifetime of the charge separated state in 95% of the mutant samples frozen under illumination was $>10^7$ s (Figure 4); the charge separated state has not decayed to the ground state in samples stored in liquid nitrogen. Thus, there is a dramatic $>10^6$-fold difference in the lifetimes of these samples.

*Light Saturation of the Inducible Signal in Samples Frozen in the Dark at 80 K.* The amplitudes of the light inducible $D^{+\bullet}$ EPR signals from native and mutant RCs frozen in the dark were measured as a function of light intensity (Figure 5) to determine the saturating level of the inducible signal. Equation 3 was fit to the measured data. For the mutant RCs, an adequate description of the observed amplitude as a function of light intensity required a minimum of two terms (Figure 5). The need for fitting with multiple terms implies a heterogeneity of the sample, that is, several subpopulations within the frozen sample.[2] In all mutant RCs, $D^{+\bullet}$ was formed in only a fraction (~30%) of the sample (Figure 5).

In the single AWM260 mutant RC, the amplitude of the light inducible EPR signal as a function of light intensity could be fit with two terms in eq 3 (Table 1). The largest term that accounts for 70% of the sample describes the majority of the population in which stable charge separation was not formed. This is a consequence of $\sigma I \Phi_B (1) \ll k_{BD}$ for this population of the sample. The second term[3] accounting for 30% of the sample describes the population in which the amplitude of the $D^{+\bullet}Q_B^{-\bullet}$ state increases with increasing light intensity. For this population, $\Phi_B (2) \sim 0.2\%$ using

[2] Heterogeneity of the illuminating light source would also result in the observed response. However, because this is not found for the native RC, we surmise that the effect is minimal and not the predominant reason for the observed heterogeneity.

[3] This term likely represents the overall result of two or more subpopulations that are not clearly discriminated under the conditions of these measurements.

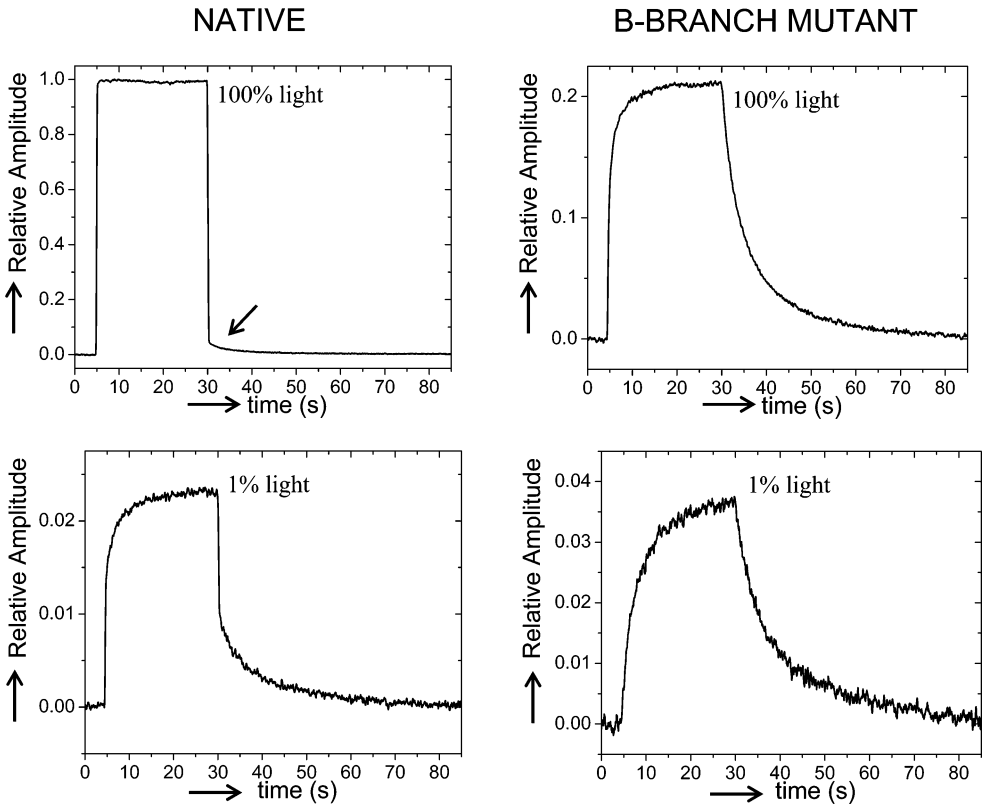


FIGURE 3: EPR signal monitored before, during, and following the illumination of dark frozen samples for the native RC (left panels) and the quintuple B-branch RCs (right panels). Shown on the top are the results of high light illumination (100%, maximum intensity) and on the bottom the results of the lower light illumination (1% of maximum intensity). Following illumination at high intensity (100%, $I \sim 0.1$ W/cm$^2$) in the native RC, the signal recovery is predominantly (95%) fast ($\tau = 30$ ms) with a small component of ~5% having a slower recovery time ($\tau = 6$ s). The faster recovery is indicative of the $D^{+\bullet}Q_A^{-\bullet} \rightarrow DQ_A$ reaction (*57*, *59*). The relative fraction of the signal with the slower recovery time is larger at lower illumination intensity (1%). In the mutant RC, the recovery of the EPR signal had no fast component, and the decay time was the same as that of the slower phase observed in the native RC ($\tau = 6$ s). During illumination at lower intensity, the EPR signal had a slower rate of formation. This result indicated that the formation occurred with low quantum efficiency due to B-branch transfer in the mutant RC and analogously attributed to B-branch transfer in the native RC (*60*). All traces were normalized to the peak amplitude of the signal of the sample frozen under illumination. (Conditions are the same as those in Figure 2; magnetic field fixed at 3211 G; field modulation $\Delta H = 1$ G; average of 10−100 traces.)

eq 4 assuming that $\Phi_A = 100\%$ at 80 K (*61*). This is within uncertainty the same as the overall value of 0.4% observed at room temperature (*10*). The light saturation curves for the LHM214/AWM260 and GDM203/AWM260 were the same (Figure 5b), indicating that within the resolution of this experiment, the predominant effect is the AWM260, which eliminates the binding of $Q_A$ (*15*, *16*).

To obtain an adequate fit of the light saturation curve of the quintuple mutant RC (Figure 5), a third term was included. The third term described a minor fraction (~20%) that had an apparently greater value for $\Phi_B$ (*3*) of ~20% (Table 1). Consequently, the fraction of $\Phi_B$ (*2*) was observed to decrease to ~10%, maintaining a value of ~30% for the sum of all active populations. Thus, the 30% active fraction appeared to be independent of the mutant system in which it was formed. The light saturation curves for the FYL181/LHM214/AWM260 was the same as that of the quintuple sample, also requiring the third term with the larger $\Phi_B$ (*3*). Thus, the fraction with the larger $\Phi_B$ (*3*) is present in mutant RCs that contain the Phe-L181 → Tyr replacement (FYL181). This enhancement of B-branch transfer was originally expected, given the observed enhancement in mutant RCs of *Rb. capsulatus* (*48*, *62*), but was not observed in the room

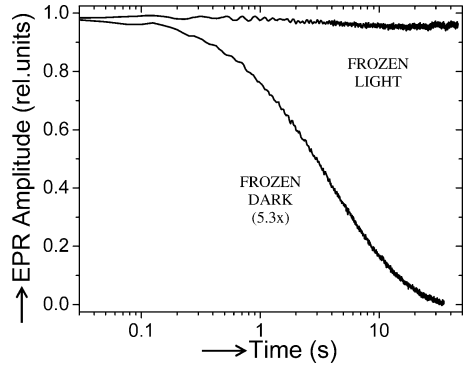


FIGURE 4: Decay of the charge separated state in the B-branch mutant RC samples. Following illumination in the frozen state, the decays of the charge separated signals were monitored using EPR spectroscopy and plotted as a function of log time. In the dark frozen sample, following illumination, the signal (Figure 3) decayed with an average time constant of ~6 s (rate constant ~0.2 s$^{-1}$); a better fit of the decay is obtained with two phases of equal amplitude and time constants of 2 and 10 s. In contrast, the charge separated state generated in the sample frozen under illumination was stable for $>10^7$ s. The amplitude of the signal from the frozen in the dark sample was increased 5.3-fold for a better comparison of the decay kinetics. (Conditions are the same as those in Figure 2.)

Table 1: Summary of Amplitudes and Quantum Efficiencies of Quinone Reduction in Native and B-Branch Mutant RCs (eqs 3 and 4)

| sample | A(1) | Φ(1) | A(2) | Φ(2) | A(3) | Φ(3) | $\tau$ (s)[a] |
|---|---|---|---|---|---|---|---|
| native [b] | 0.95 | 100% | 0.05 | ∼1% | [c] | [c] | 0.033, 6 |
| AWM260 | 0.69 | n.d.[d] | 0.31 | 0.2% | [c] | [c] | 6 |
| LHM214/AWM260 | 0.71 | n.d.[d] | 0.29 | 0.2% | [c] | [c] | 6 |
| GDM203AWM260 | 0.70 | n.d.[d] | 0.30 | 0.2% | [c] | [c] | 6 |
| FYL181/LHM214/ AWM260 | 0.71 | n.d.[d] | 0.19 | 0.3% | 0.10 | 20% | 6 |
| FYL181/GDM203/ YFM210/LHM214/ AWM260 (quintuple) | 0.71 | n.d.[d] | 0.20 | 0.3% | 0.09 | 20% | 6 |

[a] This is the average time constant for decay back to the ground state; in general, the recombination kinetics are multiphasic. [b] The quantum efficiency for forming $D^+Q_A^-$ ($\Phi_A$) was taken to be 1.0 (i.e., 100%) for the Native RC with a lifetime of 30 ms. The quantum efficiency for forming the more stable phase is ∼1% with a lifetime of 6 s. A more detailed analysis and discussion is presented elsewhere (*60*). [c] Not applicable. [d] n.d., could not be determined from the data because the charge separated state was not stably formed in this fraction of the population. The statistical error in the estimated values is ∼20%, but there is also an expected systematic error of ∼20% introduced by the assumption that the cross section is identical in the samples. Thus, the estimates are accurate to approximately a factor of 2.

temperature measurements on the *Rb. sphaeroides* mutant RCs used in this study (*10*).

In the mutant RCs investigated in this study, the total active fraction of ∼30% (extrapolated to infinite light intensity) was the same, independent of the quantum efficiencies to form $Q_B^{-\bullet}$ (Figure 5b). Thus, only a minor fraction of RCs can undergo stable charge separation at 80 K, whereas the majority cannot be trapped in a stable excited state.

For measurements made in the native RC (Figure 5), one term was used to describe the observed behavior of the fast and slow decaying phases. The slowly decaying phase was found to attain half saturation at a lower light intensity than the fast phase (Figure 5). This was due to the slower rate of recombination that allowed the accumulation of the slowly decaying state despite its lower quantum efficiency for formation (Table 1). The apparent smaller amplitude compared to that observed in the mutant RC is a consequence of competition with the formation of $D^{+\bullet}Q_A^{-\bullet}$. A more detailed description and analysis of the light induced signals observed in the native RC are presented by Paddock et al. (*60*).

## DISCUSSION

In this work, we investigated the electron transfer kinetics and EPR spectra of RC conformations trapped at low-temperature, both preceding and following $Q_B$ reduction. In the frozen state, light induced electron transfer to $Q_B$ in mutant RCs lacking $Q_A$ was attributed to B-branch electron-transfer similar to the reaction observed at room temperature (*10*, *15*). The lifetime of the $D^{+\bullet}Q_B^{-\bullet}$ state formed by freezing under illumination (after electron transfer) was $>10^6$-fold longer than that for RCs frozen in the dark (before electron transfer). This change is attributed to differences in the RC conformations between the neutral and charge separated states. We discuss below the implications of these findings on the configurations of neutral $Q_B$ and of $Q_B^{-\bullet}$ trapped at 80 K. We present a simple model to explain the experimental measurements and discuss the functional properties of $Q_B$ bound in different conformations.

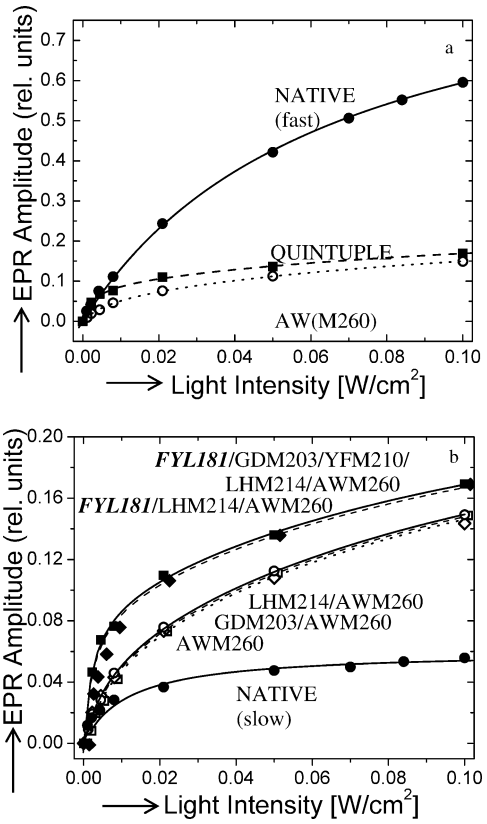


FIGURE 5: Light saturation curve of the reversible inducible signal observed in the Frozen Dark + Light sample (Figure 2). The EPR amplitude, normalized to that observed in the duplicate sample that was frozen under illumination, was measured as a function of the CW light intensity. (a) Comparison of the data for the native (●), quintuple (■), and AWM260 (○) mutant RCs. The native data were fitted (solid lines) to a single term for eq 3, to two terms for AWM260, and three terms for the quintuple (see text). The maximum possible amplitude of the active population was 1.0 (100%) in the native RC and ∼30% in both mutant RCs. (b) Comparison of different mutant RCs. The light intensity dependence can be fit with two terms for the AWM260 (○), GDM203/AWM260 (□), and LHM214/AWM260 (◇) mutant RCs. A third term was required for the ***FYL181***/LHM214/AWM260 (◆) and ***FYL181***/GDM203/YFM210/LHM214/AWM260 (■) (quintuple) RCs. This additional term was associated with the Phe-L181 → Tyr mutation (***FYL181***) introduced along the B-branch. (Conditions are the same as those in Figure 2.)

*Electron Transfer Rates of RC in Different Conformational States.* In this study, electron transfer rates were measured for RCs frozen in different states at cryogenic temperature (*5*, *43*, *63*, *64*). The charge separated state $D^{+\bullet}Q_B^{-\bullet}$ that is formed in the mutant RCs by illumination during freezing represents a relaxed configuration and is characterized by a long lifetime ($\tau > 10^7$ s). Long-lived $D^{+\bullet}Q_B^{-\bullet}$ states at low temperature were previously observed in native RC samples that were frozen under illumination. Using optical spectroscopy, Kleinfeld et al. (*5*) observed that $D^{+\bullet}$ recovered slowly with distributed nonexponential kinetics. At 80 K, a significant fraction of $D^{+\bullet}$ had not recovered during the course of the experiment ($10^4$ s). Xu et al. (*43*) observed recovery times of $D^{+\bullet}$ in the range of 10−100 s with a fraction that did not recover, attributed to samples that may have lost the electron on the acceptor side. Using EPR spectroscopy, Utshig et al. (*64*) also observed a fraction that recovered nonexponentially in 10−100 s and a fraction that was nonrecovering. The relative fraction that recovered depended on the illumination

conditions during the freezing process. Because they were able to directly observe $Q_B^{-\bullet}$ using high-field EPR spectroscopy, they could rule out the possibility that the stability of the long-lived state was due to the loss of the electron from the acceptor $Q_B^{-\bullet}$. This long-lived fraction is analogous to that found in this study in the mutant RCs. The molecular basis for the long lifetime is currently under investigation. Preliminary ENDOR studies suggest that changes in the H-bond interactions of the RC with $Q_B^{-\bullet}$ provide additional stabilization to the relaxed $D^{+\bullet}Q_B^{-\bullet}$ state (*65*).

In dark frozen mutant RCs (i.e., frozen in the neutral ground state before electron transfer), the observed heterogeneity in the rates of electron transfer indicated a distribution of conformational states. The major fraction (70%) of the sample was incapable of forming $D^{+\bullet}Q_B^{-\bullet}$ at cryogenic temperatures even at high light intensities (Table 1). This lack of activity could be due to either a slow rate of formation or a rapid decay of the excited state. The active fraction (~30%) formed $D^{+\bullet}Q_B^{-\bullet}$ upon illumination with a low quantum yield (Table 1) that was dependent on the mutations located at sites near the tetrapyrrole acceptor species. Irrespective of the quantum yield, the active fraction remained relatively constant (30%), indicating that it was determined by the properties near the $Q_B$ site, which remain unchanged by the mutations (see below). In addition, the lifetime of the charge separated $D^+Q_B^-$ state was the same ($\tau = 6$ s) for all mutant RCs (Table 1). Surprisingly, a small component of the EPR signal observed in the native RC had the same lifetime of 6 s (Figure 3). The EPR signal showed a slowly rising component during illumination at lower intensities (Figure 3), indicating a low quantum yield for formation (Table 1). Additional properties of this component led to its assignment to a small fraction of RCs that reduce $Q_B$ *via* low efficiency B-branch electron transfer in the native RC (*60*). The identity of the 6 s time constants observed in RCs lacking $Q_A$ and in the native RC indicates that the mutations have not altered the direct tunneling reaction between $D^{+\bullet}$ and $Q_B^{-\bullet}$. Thus, the environments around $D^{+\bullet}$ and $Q_B^{-\bullet}$ are substantially unchanged by B-branch mutations.

In previous studies, native RCs frozen under illumination displayed a distribution of lifetimes for the charge separated states ranging from 10 s to $>10^4$ s (*5*, *43*, *64*). In native RCs, the reduction of $Q_B$ occurs almost exclusively by electron transfer from $Q_A^{-\bullet}$. Because this transfer is fast and reversible, the electron hops between the two quinones during the freezing process. Thus, the protein structure surrounding $Q_B$ may be affected by the details of competing processes, such as protein relaxation, electron transfer, and freezing. Therefore, the native RC sample frozen under illumination may have structures intermediate between the relaxed and the unrelaxed structures. States with longer lifetimes would have structures that resemble the relaxed state. States with shorter lifetimes would have structures that resemble the unrelaxed state. This model qualitatively explains the distribution of lifetimes spanning many orders of magnitude. The distribution of rates is due to different protein conformational states that lie along the reaction coordinate leading from the neutral ($DQ_B$), in the unrelaxed state, to the fully relaxed charge separated state ($D^{+\bullet}Q_B^{-\bullet}$) (*5*, *43*). The lifetimes measured in the present work on mutant RCs can be explained by this model. In dark frozen (unrelaxed) mutant RCs, the measured lifetime ($\tau$ ~6 s) is shorter than the lifetimes measured in native RCs frozen under illumination ($\tau > 10$ s), consistent with a totally unrelaxed state. In mutant RCs frozen in the light (relaxed), the long lifetime ($\tau > 10^7$ s) is consistent with the lifetime of a totally relaxed state. The absence of $Q_A$ eliminates electron hopping from $Q_B^{-\bullet}$ in these mutant RCs, thereby constraining the RC to be in the $D^{+\bullet}Q_B^{-\bullet}$ state when illuminated during the freezing process. Thus, the conformational states found in the present study that are formed by freezing in the dark and in the light can be considered to be the initial and final states along the reaction path for electron transfer.

*Molecular Basis for the Heterogeneity at the Quinone ($Q_B$) Binding Site.* The data show that there are several distinct quinone ($Q_B$) states as well as distinct conformational states of the surrounding protein. In all mutant RCs, the total fraction of the sample that was activated in the dark frozen sample upon illumination was ~30%. The fraction was independent of the quantum efficiency of formation, indicating that it is an intrinsic property of the acceptor ($Q_B$) site. Because the crystal structures of the RCs show two distinct binding positions (*26*−*30*), proximal and distal to the nonheme $Fe^{2+}$, the observed behavior likely reflects this distribution in the quinone binding positions. Below, we discuss the rationale for assigning the different conformational states.

*Conformational Assignments of the $Q_B$ States in the Mutant RCs.* The minor (~30%) active population capable of $Q_B$ reduction in the sample frozen in the dark (unrelaxed conformation) is assigned to the fraction of RCs having a proximal $Q_B$ ($DH_BQ_B(p)$) for the following reasons: (1) the relatively long lifetime of $Q_B^{-\bullet}$ formed by illumination indicates stabilization of $Q_B^{-\bullet}$ by H-bonds as is found in illuminated RC samples and crystals (*27*, *28*, *32*); (2) there is no contribution of an uncoupled $Q_B^{-\bullet}$ EPR signal to the observed spectrum indicating a broadening of the $Q_B^{-\bullet}$ signal because of its close proximity to the high spin $Fe^{2+}$; and (3) preliminary ENDOR spectroscopy indicated that the photochemically active $Q_B$ is in the proximal site (*65*) (to be presented in further detail in a subsequent publication). Upon illumination at low temperature, we form the charge separated state $D^{+\bullet}H_BQ_B^{-\bullet}(p)^U$ in RCs with proximal $Q_B$. The relatively rapid charge recombination time ($\tau = 6$ s) compared to that of the light frozen sample is due to the higher energy of this state due to the absence of stabilizing protein and solvent relaxation.[4] These findings are in agreement with FTIR measurements made in frozen samples of a B-branch mutant, in which a similar minor fraction (~10%) of the dark frozen sample could undergo stable charge separation (*66*). The larger value of ~30% reported in this work is the hypothetical maximum fraction observed only at infinite light intensity.

The larger (70%) inactive population in RCs frozen in the dark is assigned to the fraction in the distal state $DH_BQ_B(d)$, based predominantly on the mutant crystal structure of the quintuple RC in which the majority of $Q_B$ is in the distal site (*10*). The lack of reactivity for the distal $Q_B$ can be explained by a higher energy of the charge separated state due to a lack of the strong H-bonds to both carbonyl oxygen atoms present in the proximal site. Alternatively, the lack

[4] To first order, we treat two $Q_B^{-\bullet}$ states as approximately the same because their recombination rates differ by ~4-fold, that is orders of magnitude less than the $>10^6$-fold difference observed between samples frozen in the light and those frozen in the dark.

of reactivity of the distal $Q_B$ may result from a weaker electronic coupling to $H_B$. However, the structural position of the quinone in the distal site is closer to $H_B$ (*10*), which would be expected to increase coupling (*67*, *68*). The relative occupancy of $Q_B$ in the two binding sites in the frozen sample, that is, 3:1 for the distal/proximal ratio, indicates only a modest difference in the binding energy ($\sim$1.5 $k_BT$) between the two sites. Because binding to these two sites is nearly isoenergetic, small changes in the binding free energy resulting from temperature or external solvent could lead to a change in the relatively occupancy. This may be one reason for the reported differences in the binding position of $Q_B$ (*26*−*30*, *69*) and the FTIR observation that $Q_B$ prefers to bind at the proximal position at room temperature (*46*).

The conformation of RCs frozen in the light, in the charge separated state, is assigned to the proximal relaxed state $D^{+\bullet}H_BQ_B^{-\bullet}(p)^R$ in which solvent relaxation that stabilizes charge separation has occurred. The EPR properties of this sample were similar to those of the light induced signals for $D^{+\bullet}H_BQ_B^{-\bullet}(p)^U$ discussed above. In addition, the larger signal from this sample allowed the observation of a broad $g = 1.82$ signal (not shown), characteristic of the $Q_B^{-\bullet}Fe^{2+}$ coupled complex in native RCs (*58*). This indicates that $Q_B^{-\bullet}$ formed by B-branch electron transfer is located at the proximal site, as it is in native RCs, as shown by X-ray crystallography (*27*, *28*) and EPR and ENDOR spectroscopy (*32*). The protein response results in the dramatic $>10^6$-fold increase in the lifetime (stability) at 80 K compared to that in the $D^{+\bullet}H_BQ_B^{-\bullet}(p)^U$ state.

*Model for the Observed Kinetic Properties.* The simplest model to explain the results (Figure 6) assumes four possible RC configurations of the quinone in the protein. The quinone may be either in the distal (d) or proximal (p) position and the protein in either an unrelaxed state (U) or a relaxed state (R) in which protein and solvent dipoles have oriented to stabilize the charge on $Q_B^{-\bullet}$. In the dark (ground state) sample, a majority ($\sim$ 70%) of the RCs are in the distal $DH_BQ_B(d)$ state that is photochemically inactive, that is, stable charge separation does not occur. In the remaining $\sim$30% of the RCs, $Q_B$ is in the proximal position (see next section), where the RCs are photochemically active, allowing the formation of the $D^{+\bullet}H_BQ_B^{-\bullet}(p)^U$ state. In the sample frozen under illumination, the states can interconvert prior to freezing, resulting in the $D^{+\bullet}H_BQ_B^{-\bullet}(p)^R$ relaxed state. The relaxation lowers the energy of the charge separated state so that appreciable charge recombination does not occur at 80 K. In the frozen state, the different configurations cannot interconvert. Electron transfer that occurs in the dark frozen RC results in formation of the unrelaxed $D^{+\bullet}H_BQ_B^{-\bullet}(p)^U$ state with an average charge recombination rate $k_{BD}{}^U \cong 0.2\ s^{-1}$ ($\tau = 6$ s), that is, $>10^6$-fold faster than that of the relaxed state $D^{+\bullet}H_BQ_B^{-\bullet}(p)^R$.

*Functional Properties of Quinone ($Q_B$) Bound at the Different Sites.* Of the four possible $Q_B$ and protein configurations, only the states involving $Q_B$ bound at the proximal site are observed (Figure 6). Although the occupancy of the distal site $DH_BQ_B(d)$ is significant at low temperature, stable charge separation to form the hypothetical $D^{+\bullet}H_BQ_B^{-\bullet}(d)^U$ state was not observed. This (lack of) observation indicates that $\sigma I\Phi_B \ll k_{BD}$, that is, either its formation was unfavorable or its lifetime was not long enough to be observed. Likewise, the hypothetical $D^{+\bullet}H_BQ_B^{-\bullet}(\mathbf{d})^R$ state is less favored than

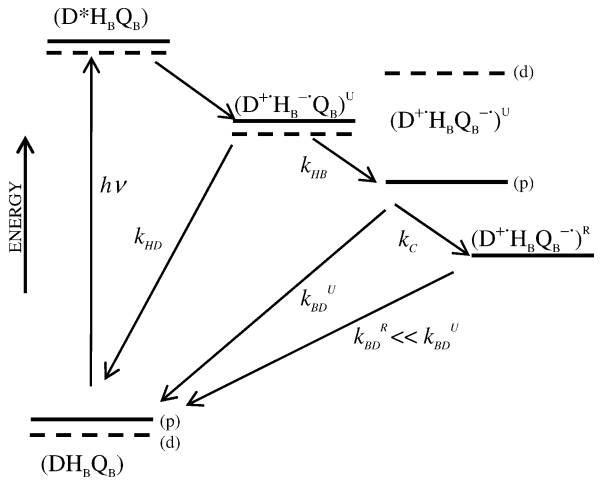


FIGURE 6: Proposed energy level diagram of the ground and charge separated states consistent with the experimental results of this work (80 K). The $DH_BQ_B$ is the ground state in one of two protein configurations with $Q_B$ in either the distal (d) (dashed lines) or proximal (p) (solid lines) sites, respectively. $D^{+\bullet}H_BQ_B^{-\bullet}(p)^U$ and $D^{+\bullet}H_BQ_B^{-\bullet}(p)^R$ are the two observed charge separated states in which $Q_B^{-\bullet}$ is formed in the proximal site with the surrounding protein either in the unrelaxed (U) or the relaxed (R) configuration, respectively. $k_{HD}$ and $k_{BD}{}^U$ are the recombination rate constants as indicated, and $k_C$ is the rate constant of the protein relaxation. Light excitation of the ground state resulting in the formation of $D^*H_BQ_B$ and electron transfer to form $D^{+\bullet}H_B^{-\bullet}Q_B$. In the dark frozen RCs, electron transfer occurs in a minor population to $Q_B(p)$ forming $D^{+\bullet}H_BQ_B^{-\bullet}(p)^U$ (*47*; subsequent publication). In contrast, electron transfer to $Q_B(d)$ is not observed, suggesting that $D^{+\bullet}H_BQ_B^{-\bullet}(d)^U$ has a higher energy. Conversion to the final relaxed $D^{+\bullet}H_BQ_B^{-\bullet}(p)^R$ occurs at room temperature but is impaired at low temperatures (e.g., 80 K). The slower charge recombination from the relaxed state $k_{BD}{}^R \ll k_{BD}{}^U$ is attributed to charge stabilization due to protein and water relaxation.

$D^{+\bullet}H_BQ_B^{-\bullet}(\mathbf{p})^R$ and is, therefore, also not observed. The change in the free energy of reduction of $Q_B$ at the two different sites was estimated from electrostatic computations to be $\sim$250 meV higher for quinone bound to the distal site than that to the proximal site (*70*). This is consistent with our observations because the population of $D^{+\bullet}H_BQ_B^{-\bullet}(d)^R$ would be too small to observe.

One of the active $Q_B$ states is $DH_BQ_B(p)^U$. Its corresponding charge separated state $D^{+\bullet}H_BQ_B^{-\bullet}(p)^U$ can be observed with an observed lifetime of $\sim$6 s ($k_{BD}{}^U \cong 0.2\ s^{-1}$). This charge separated state must have a free energy below that of $D^{+\bullet}H_B^{-\bullet}Q_B(p)$ because its formation is favorable. The other active $Q_B$ state is $D^{+\bullet}H_BQ_B^{-\bullet}(p)^R$, which had the greatest lifetime ($\tau > 10^7$ s; 80 K). The long lifetime is due to stabilization of the charge separated state *via* the protein response. At 80 K, the protein response is frozen in the sample, resulting in the $>10^7$ s lifetime. Consequently, we did not observe the $DH_BQ_B(p)^R$ state in which the electron moves back to the oxidized donor. Long-lived states were previously observed in both optical (*5*, *43*) and EPR spectroscopic studies (*64*).

The increased stability of the relaxed state compared to that of the unrelaxed state is not a consequence of the different binding position of $Q_B^{-\bullet}$ (see section above); therefore, it must be due to other changes, such as protonation and H-bonding. It has been proposed from electro-

static computations that the hydroxyl group of Ser-L223 reorients and forms a stabilizing H-bond to $Q_B^{-\bullet}$. Coupled to this reorientation is the protonation (neutralization) of a nearby Asp-L213 (*70*−*72*). These changes could provide sufficient free energy to account for the observed effects at 80 K. We are in the process of experimentally investigating the molecular differences using ENDOR spectroscopy. The results of this study are the subject of a subsequent publication.

*Conformational Gate.* One of the remaining unknown steps related to RC function is the identification of the conformational gate that limits the observed rate for the first electron transfer. The existence of different protein conformations with very different characteristics was shown by the inhibition of electron transfer from $Q_A^{-\bullet}$ to $Q_B$ in RCs frozen in the dark (*4*, *5*); this was in contrast to viable electron transfer in RCs frozen under illumination. Subsequently, several studies to investigate these conformers (i.e., substates) were performed and the properties of charge separation investigated (*43*, *73*). These states have been proposed in a general sense to differ in the detailed interactions between $Q_B$ and the protein. Electrostatic interactions have been shown to be of functional importance. In response to charge separation, amino acid groups change their states of protonation resulting in a net proton uptake (*35*, *36*). The different protonation states are one contribution to the relative energy of these substates (*37*, *38*, *74*). Although some of the molecular details have been proposed from computational work (*38*, *70*, *72*), experimental testing and verification of the molecular interactions have just recently been initiated (*65*).

Our results are consistent with the simple model for the conformationally gated electron transfer presented in eq 5

$$Q_A^{-\bullet}Q_B(d) \rightleftharpoons Q_A^{-\bullet}Q_B(p) \xrightarrow{k_C} (Q_A^{-\bullet}Q_B) \xrightarrow{k_{et(1)}} (Q_AQ_B^{-\bullet}) \qquad (5)$$

where $k_{AB}^{(1)}$ is the rate constant of the rate-limiting conformational gate (*9*), $k_{et(1)}$ is the intrinsic electron transfer rate constant, $(Q_A^{-\bullet}Q_B)$ is the intermediate state, and $Q_A^{-\bullet}Q_B(d)$ and $Q_A^{-\bullet}Q_B(p)$ are the initial states with $Q_B$ in the distal (d) or proximal (p) location, respectively. The energy of this intermediate state lies above that of the two initial states as well as the final $(Q_AQ_B^{-\bullet})$ state. In particular, our results show that $Q_B^{-\bullet}(d)$ cannot be stably formed, confirming the necessity for $Q_B$ to move into the proximal position for stabilization (*27*). Furthermore, our results show that a significant protein response is required to stabilize $(Q_AQ_B^{-\bullet})$. Although our results do not imply that the movement of quinone from the distal to proximal sites is rate-limiting, they do support the idea that the movement to the proximal site is a necessary prerequisite for its stabilization (*27*).

The unrelaxed state $D^{+\bullet}H_BQ_B^{-\bullet}(p)^U$ (Figure 5) trapped in this work is sufficiently high in energy that it is not accessible *via* electron transfer from $Q_A^{-\bullet}$, the physiological electron donor in the native RC. Thus, it is most likely that the structural changes that occur in the conformational gate step of electron transfer to form $(Q_AQ_B^{-\bullet})$ (eq 5) also occur in forming the $D^{+\bullet}H_BQ_B^{-\bullet}(p)^R$ state. In other words, the molecular changes that occur during the conformational gate step are reflected in the structural differences between the initial $D^{+\bullet}H_BQ_B^{-\bullet}(p)^U$ state and the final relaxed state $D^{+\bullet}H_BQ_B^{-\bullet}(p)^R$ observed in this work. Therefore, we consider the determination of the molecular differences between $D^{+\bullet}H_BQ_B^{-\bullet}(p)^U$ and $D^{+\bullet}H_BQ_B^{-\bullet}(p)^R$ to be of fundamental importance in understanding the reaction mechanism and are using ENDOR spectroscopy to investigate these differences.

## ACKNOWLEDGMENT

We thank George Feher for helpful discussions and the reviewers of this article who made it better by their critical comments.

## REFERENCES

1. Marcus, R. A., and Sutin, N. (1985) Electron transfer in chemistry and biology, *Biochim. Biophys. Acta 811*, 265−322.
2. Hoffman, B. M., and Ratner, M. A. (1987) Gated electron transfer: when are observed rates controlled by conformational interconversion? *J. Am. Chem. Soc. 109*, 6237−6242.
3. Sharp, R. E., and Chapman, S. K. (1999) Mechanisms for regulating electron transfer in multi-centre redox proteins, *Biochim. Biophys. Acta 1432*, 143−158.
4. Chamorovsky, S. K., Remennikov, S. M., Kononenko, A. A., Venediktov, P. S., and Rubin, A. B. (1976) New experimental approach to the estimation of rate of electron transfer from the primary to secondary acceptors in the photosynthetic electron transport chain of purple bacteria, *Biochim. Biophys. Acta*. *430*, 62−70.
5. Kleinfeld, D., Okamura, M. Y., and Feher, G. (1984) Electron-transfer kinetics in photosynthetic reaction centers cooled to cryogenic temperatures in the charge-separated state: evidence for light-induced structural changes, *Biochemistry 23*, 5780−5786.
6. Noks, P. P., Lukashev, E. P., Kononenko, A. A., Venediktov, P. S., and Rubin, A. B. (1977) Possible role of macromolecular components in functioning of photosynthetic reaction centers of purple bacteria. *Mol. Biol. 11*, 835−842.
7. Francia, F., Palazzo, G., Mallardi, A., Cordone, L., and Venturoli, G. (2003) Residual water modulates $Q_A^-$-to-$Q_B$ electron transfer in bacterial reaction centers embedded in trehalose amorphous matrices, *Biophys. J. 85*, 2760−2775.
8. Francia, F., Giachini, L., Palazzo, G., Mallardi, A., Boscherini, F., and Venturoli, G. (2004) Electron transfer kinetics in photosynthetic reaction centers embedded in polyvinyl alcohol films, *Bioelectrochemistry 63*, 73−77.
9. Graige, M. S., Feher, G., and Okamura, M. Y. (1998) Conformation gating of the electron transfer reaction $Q_A^{-\bullet}Q_B \rightarrow Q_AQ_B^{-\bullet}$, in bacterial reaction centers of *Rb. sphaeroides* determined by a driving force assay, *Proc. Natl. Acad. Sci. U.S.A. 95*, 11679−11684.
10. Paddock, M. L., Chang, C., Xu, Q., Abresch, E. C., Axelrod, H. L., Feher, G., and Okamura, M. Y. (2005) Quinone (QB) reduction by B-branch electron transfer in mutant bacterial reaction centers from *Rhodobacter sphaeroides*: quantum efficiency and X-ray structure, *Biochemistry 44*, 6920−6928.
11. Heller, B. A., Holten, D., and Kirmaier, C. (1995) Control of electron transfer between the L- and M-sides of photosynthetic reaction centers, *Science 269*, 940−945.
12. Kirmaier, C., Laible, P. D., Hanson, D. K., and Holten, D. (2003) B-side charge separation in bacterial photosynthetic reaction centers: nanosecond time scale electron transfer from $H_B^-$ to $Q_B$, *Biochemistry 42*, 2016−2024.
13. Blankenship, R. E., Madigan, M. T., and Bauer, C. E. (1995) *Anoxygenic Photosynthetic Bacteria*, Vol. 2, Kluwer Academic Publishers, Dordrecht, The Netherlands.
14. Blankenship, R. E. (2002) *Molecular Mechanisms of Photosynthesis*, Blackwell Science, Inc., London.
15. Ridge, J. P., van Brederode, M. E., Goodwin, M. G., van Grondelle, R., and Jones, M. R. (1999) Mutations that modify or exclude binding of the $Q_A$ ubiquinone and carotenoid in the reaction center from *Rhodobacter sphaeroides*, *Photosynth Res. 59*, 9−26.
16. McAuley, K. E., Fyfe, P. K., Ridge, J. P., Cogdell, R. J., Isaacs, N. W., and Jones, M.R. (2000) Ubiquinone binding, ubiquinone exclusion, and detailed cofactor conformation in a mutant bacterial reaction center, *Biochemistry 39*, 15032−15043.
17. Kirmaier, C., Gaul, D., DeBey, R., Holten, D., and Schenck, C. C. (1991) Charge separation in a reaction center incorporating

bacteriochlorophyll for photoactive bacteriopheophytin, *Science 251*, 922−927.
18. Feher, G., Allen, J. P., Okamura, M. Y., and Rees, D. C. (1989) Structure and function of bacterial photosynthetic reaction centers, *Nature 339*, 111−116.
19. Hoff, A. J., and Deisenhofer, J. (1997) Photophysics of photosynthesis: structure and spectroscopy of reaction centers of purple bacteria, *Phys. Rep. 287*, 2−247.
20. Okamura, M. Y., and Feher, G. (1992) Proton transfer in reaction centers from photosynthetic bacteria, *Annu. Rev. Biochem. 61*, 861−896.
21. Vermeglio, A. (1977) Secondary electron transfer in reaction centers of *Rhodopseudomonas sphaeroides*. Out-of-phase periodicity of two for the formation of ubisemiquinone and fully reduced ubiquinone, *Biochim. Biophys. Acta 459*, 516−524.
22. Tiede, D. M., Vazquez, J., Cordova, J., and Marone, P. A. (1996) Time-resolved electrochromism associated with the formation of quinone anions in the *Rhodobacter sphaeroides* R26 reaction center, *Biochemistry 35*, 10763−10775.
23. Li, J., Gilroy, D., Tiede, D. M., and Gunner, M. R. (1998) Kinetic phases in the electron transfer from $P^+Q_A^-Q_B$ to $P^+Q_AQ_B^-$ and the associated processes in *Rhodobacter sphaeroides* R-26 reaction centers, *Biochemistry 37*, 2818−2829.
24. Mulkidjanian, A. Y., Kozlova, M. A., and Cherepanov, D. A. (2005) Ubiquinone reduction in the photosynthetic reaction centre of *Rhodobacter sphaeroides*: interplay between electron transfer, proton binding and flips of the quinone ring, *Biochem. Soc. Trans. 33*, 845−850.
25. Lancaster, C. R., and Michel, H. (1997) The coupling of light-induced electron transfer and proton uptake as derived from crystal structures of reaction centres from *Rhodopseudomonas viridis* modified at the binding site of the secondary quinone, $Q_B$, *Structure 5*, 1339−1359.
26. Ermler, U., Fritzsch, G., Buchanan, S. K., and Michel, H. (1994) Structure of the photosynthetic reaction centre from *Rhodobacter sphaeroides* at 2.65 Å resolution: cofactors and protein-cofactor interactions, *Structure 2*, 925−936.
27. Stowell, M. H., McPhillips, T. M., Rees, D. C., Soltis, S. M., Abresch, E., and Feher, G. (1997) Light-induced structural changes in photosynthetic reaction center: implications for mechanism of electron-proton transfer, *Science 276*, 812−816.
28. Fritzsch, G., Koepke, J., Diem, R., Kuglstatter, A., and Baciou, L. (2002) Charge separation induces conformational changes in the photosynthetic reaction centre of purple bacteria, *Acta Crystallogr., Sect. D 58*, 1660−1663.
29. Kuglstatter, A., Ermler, U., Michel, H., Baciou, L., and Fritzsch, G. (2001) X-ray structure analyses of photosynthetic reaction center variants from *Rhodobacter sphaeroides*: structural changes induced by point mutations at position L209 modulate electron and proton transfer, *Biochemistry 40*, 4253−4260.
30. Pokkuluri, P. R., Laible, P. D., Crawford, A. E., Mayfield, J. F., Yousef, M. A., Ginell, S. L., Hanson, D. K., and Schiffer, M. (2004) Temperature and cryoprotectant influence secondary quinone binding position in bacterial reaction centers, *FEBS Lett. 570*, 171−174.
31. Isaacson, R. A., Abresch, E. C., Lendzian, F., Boullais, C., Paddock, M. L., Mioskowski, C., Lubitz, W., and Feher, G. (1996) Asymmetry of the Binding Sites of $Q_A^{-\bullet}$ and $Q_B^{-\bullet}$ in Reaction Centers of *Rb. sphaeroides* Probed by Q-Band EPR with $^{13}C$-Labeled Quinones, in *The Reaction Center of Photosynthetic Bacteria, Structure and Dynamics* (Michel-Beyerle, M.-E., Ed.) pp. 353−367, Springer-Verlag, Berlin, Germany.
32. Lubitz, W., and Feher, G. (1999) The primary and secondary acceptors in bacterial photosynthesis: III Characterization of the quinone radicals $Q_A^{-\bullet}$ and $Q_B^{-\bullet}$ by EPR and ENDOR, *Appl. Magn. Reson. 17*, 1−48.
33. Breton, J., Wakeham, M. C., Fyfe, P. K., Jones, M. R., and Nabedryk, E. (2004) Characterization of the bonding interactions of Q(B) upon photoreduction via A-branch or B-branch electron transfer in mutant reaction centers from *Rhodobacter sphaeroides*, *Biochim. Biophys. Acta 1656*, 127−138.
34. Brudler, R., de Groot, H. J. M., van Liemt, W. B. S., Gast, P., Hoff, A. J., Lugtenburg, J., and Gerwert, K. (1995) FTIR spectroscopy shows weak symmetric hydrogen bonding of the $Q_B$ carbonyl groups in *Rhodobacter sphaeroides* R26 reaction centres, *FEBS Lett. 370*, 88−92.
35. McPherson, P. H., Okamura, M. Y., and Feher, G. (1988) Light-induced proton uptake by photosynthetic reaction centers from *Rhodobacter sphaeroides* R-26, I. Protonation of the one-electron states $D^+Q_A^-$, $DQ_A^-$, $D^+Q_AQ_B^-$, and $DQ_AQ_B^-$, *Biochim. Biophys. Acta 934*, 348−368.
36. Maroti, P., and Wraight, C. A. (1988) Flash-induced HI binding by bacterial photosynthetic reaction centers: influences of the redox states of the acceptor quinones and primary donor, *Biochim. Biophys. Acta 934*, 329−347.
37. Beroza, P., Fredkin, D. R., Okamura, M. Y., and Feher, G. (1995) Protonation of interacting residues in a protein by a Monte Carlo method: application to lysozyme and the photosynthetic reaction center of *Rhodobacter sphaeroides*. *Proc. Natl. Acad. Sci. U.S.A. 88*, 5804−5808.
38. Alexov, E. G., and Gunner, M. R. (1997) Incorporating protein conformational flexibility into the calculation of pH-dependent protein properties, *Biophys. J. 72*, 2075−2093.
39. Hienerwadel, R., Grzybek, S., Fogel, C., Kreutz, W., Okamura, M. Y., Paddock, M. L., Breton, J., Nabedryk, E., and Mäntele, W. (1995) Protonation of Glu L212 following $Q_B^-$ formation in the photosynthetic reaction center of Rhodobacter sphaeroides: Evidence from time-resolved infrared spectroscopy, *Biochemistry 34*, 2832−2843.
40. Nabedryk, E., Breton, J., Hienerwadel, R., Fogel, C., Mäntele, W., Paddock, M. L., and Okamura, M. Y. (1995) Fourier transform infrared difference spectroscopy of secondary quinone acceptor photoreduction in proton transfer mutants of *Rhodobacter sphaeroides*, *Biochemistry 34*, 14722−14732.
41. McComb, J. C., Stein, R. R., and Wraight, C. A. (1990) Investigations on the influence of headgroup substitution and isoprene side-chain length in the function of primary and secondary quinones of bacterial reaction centers, *Biochim. Biophys. Acta 1015*, 156−171.
42. Xu, Q., Baciou, L., Sebban, P., and Gunner, M. R. (2002) Exploring the energy landscape for Q(A)(-) to Q(B) electron transfer in bacterial photosynthetic reaction centers: effect of substrate position and tail length on the conformational gating step, *Biochemistry 41*, 10021−10025.
43. Xu, Q., and Gunner, M. R. (2001) Trapping conformational intermediate states in the reaction center protein from photosynthetic bacteria, *Biochemistry 40*, 3232−3241.
44. Laible, P. D., Kirmaier, C., Udawatte, C. S., Hofman, S. J., Holten, D., and Hanson, D. K. (2003) Quinone reduction via secondary B-branch electron transfer in mutant bacterial reaction centers, *Biochemistry 18*, 1718−1730.
45. Wakeham, M. C., Goodwin, M. G., McKibbin, C., and Jones, M. R. (2003) Photo-accumulation of the $P^+Q_B^-$ radical pair state in purple bacterial reaction centres that lack the $Q_A$ ubiquinone, *FEBS Lett. 540*, 234−240.
46. Breton, J. (2004) Absence of large-scale displacement of quinone $Q_B$ in bacterial photosynthetic reaction centers, *Biochemistry 43*, 3318−3326.
47. Paddock, M. L., Flores, M., Isaacson, R. I. Chang, C., Abresch, E. C., Selvaduray, P., Feher, G., and Okamura, M. Y. (2005) $Q_B^{-\bullet}$ Formation by B-Branch Electron Transfer in Reaction Centers from *Rhodobacter sphaeroides*, in *Photosynthesis: Fundamental Aspects to Global Perspectives*, (van der Est, A., and Bruce, D., Eds.) pp 207−209, Alliance Communications Group, Lawrence, KS.
48. Kirmaier, C., He, C., and Holten, D. (2001) Manipulating the direction of electron transfer in the bacterial reaction center by swapping Phe for Tyr near $BChl_M$ (L181) and Tyr for Phe near $BChl_L$ (M208), *Biochemistry 40*, 12132−12139.
49. Williams, J. C., Alden, R. G., Murchison, H. A., Peloquin, J. M., Woodbury, N. W., and Allen, J. P. (1992) Effects of mutations near the bacteriochlorophylls in reaction centers from *Rhodobacter sphaeroides*, *Biochemistry 31*, 11029−11037.
50. de Boer, A. L., Neerken, S., de Wijn, R., Permentier, H. P., Gast, P., Vijgenboom, E., and Hoff, A. J. (2002) High yield of B-branch electron transfer in a quadruple reaction center mutant of the photosynthetic bacterium Rhodobacter sphaeroides, *Biochemistry 41*, 3081−3088.
51. de Boer, A. L., Neerken, S., de Wijn, R., Permentier, H. P., Gast, P., Vijgenboom, E., and Hoff, A. J. (2002) B-branch electron transfer in reaction centers of Rhodobacter sphaeroides assessed with site-directed mutagenesis, *Photosynth. Res. 71*, 221−239.
52. Kirmaier, C., Cua, A., He, C., Holten, D., and Bocian, D. F. (2002) Probing M-branch electron transfer and cofactor environment in the bacterial photosynthetic reaction center by addition of a hydrogen bond to the M-side bacteriopheophytin, *J. Phys. Chem. B 106*, 495−503.

53. Kirmaier, C., Laible, P. D., Czarnecki, K., Hata, A. N., Hanson, D. K., Bocian, D. F., and Holten, D. (2002) Comparison of M-side electron transfer in *Rb. sphaeroides* and *Rb. capsulatus* reaction centers, *J. Phys. Chem. B 106*, 1799−1808.
54. Paddock, M. L., Isaacson, R., Chang, C., Feher, G., and Okamura, M. Y. (2004) Conformations of $Q_B^{-\bullet}$ trapped by B side electron transfer in reaction centers from *Rhodobacter sphaeroides*, *Biophys. J. 86*, 11a.
55. Paddock, M. L., Rongey, S. H., Abresch, E. C., Feher, G., and Okamura, M. Y. (1988) Reaction centers from three herbicide resistant mutants of *Rhodobacter sphaeroides* 2.4.1: Sequence analysis and preliminary characterization, *Photosynth. Res. 17*, 75−96.
56. Calvo, R., Abresch, E. C., Bittl, R., Feher, G., Hofbauer, W., Isaacson, R. A., Lubitz, W., Okamura, M. Y., and Paddock, M. L. (2000) EPR study of the molecular and electronic stucture of the semiquinone biradical $Q_A^{-\bullet}$ $Q_B^{-\bullet}$ in photosynthetic reaction centers from *Rb. sphaeroides*, *J. Am. Chem. Soc. 122*, 7327−7341.
57. McElroy, J. D., Feher, G., and Mauzerall, D. C. (1972) Characterization of primary reactants in bacterial photosynthesis. I. Comparison of the light-induced EPR signal (g = 2.0026) with that of a bacteriochlorophyll radical, *Biochim. Biophys. Acta 267*, 363−374.
58. Butler, W. F., Calvo, R., Fredkin, D. R., Isaacson, R. A., Okamura, M. Y., and Feher, G. (1984) The electronic structure of $Fe^{2+}$ in reaction centers from *Rhodopseudomonas sphaeroides* III. EPR measurements of the reduced acceptor complex, *Biophys. J. 45*, 947−973.
59. Feher, G., Isaacson, R. A., Ackerson, L. C., and Okamura, M. Y. (1974) On the question of the primary acceptor in bacterial photosynthesis: Manganese substituting for iron in reaction centers of *Rhodopseudomonas spheroides* R-26, *Biochim. Biophys. Acta 368*, 135−139.
60. Paddock, M. L., Isaacson, R. A., Abresch, E. C., and Okamura, M. Y. (2006) Light induced EPR spectra of reaction centers from *Rhodobacter sphaeroides* at 80K: Evidence for reduction of $Q_B$ by B-branch electron transfer in native reaction centers, *Appl. Magn. Reson.*, in press.
61. Clayton, R. K., and Yamamoto, T. (1976) Photochemical quantum efficiency and absorption spectra of reaction centers from *Rhodopseudomonas sphaeroides* at low temperature, *Photochem. Photobiol. 26*, 67−70.
62. Chuang, J. I., Boxer, S. G., Holten, D., and Kirmaier, C. (2006) High yield of M-side electron transfer in mutants of *Rhodobacter capsulatus* reaction centers lacking the L-side bacteriopheophytin, *Biochemistry 45*, 3845−3851.
63. McMahon, B. H., Muller, J. D., Wraight, C. A., and Nienhaus, G. U. (1998) Electron transfer and protein dynamics in the photosynthetic reaction center, *Biophys. J. 74*, 2567−2587.
64. Utschig, L. M., Thurnauer, M. C., Tiede, D. M., and Poluektov, O. G. (2005) Low-temperature interquinone electron transfer in photosynthetic reaction centers from Rhodobacter sphaeroides and Blastochloris viridis: characterization of Q(B)- states by high-frequency electron paramagnetic resonance (EPR) and electron-nuclear double resonance (ENDOR), *Biochemistry 44*, 14131−14142.
65. Paddock, M. L., Flores, M., Isaacson, R., Chang, C., Selvaduray, P., Feher, G., and Okamura, M. Y. (2005) Hydrogen bond reorientation upon $Q_B^{-\bullet}$ formation revealed by ENDOR spectroscopy in reaction centers from *Rhodobacter sphaeroides*, *Biophys. J. 88*, A204.
66. Wakeham, M. C., Breton, J., Nabedryk, E., and Jones, M. R. (2004) Formation of a semiquinone at the $Q_B$ site by A- or B-branch electron transfer in the reaction center from *Rhodobacter sphaeroides*, *Biochemistry 43*, 4755−4763.
67. Noy, D., Moser, C. C., and Dutton, P. L. (2006) Design and engineering of photosynthetic light-harvesting and electron transfer using length, time, and energy scales, *Biochim. Biophys. Acta 1757*, 90−105.
68. Tan, M. L., Balabin, I., and Onuchic, J. N. (2004) Dynamics of electron transfer pathways in cytochrome C oxidase, *Biophys. J. 86*, 1813−1819.
69. Xu, Q., Axelrod, H. L., Abresch, E. C., Paddock, M. L., Okamura, M. Y., and Feher, G. (2004) X-ray structure determination of three mutants of the bacterial photosynthetic reaction centers from *Rb. sphaeroides*: Altered proton transfer pathways, *Structure 12*, 703−715.
70. Zhu, Z., and Gunner, M. R. (2005) Energetics of quinone-dependent electron and proton transfers in *Rhodobacter sphaeroides* photosynthetic reaction centers, *Biochemistry 44*, 82−96.
71. Alexov, E. G., and Gunner, M. R. (1999) Calculated protein and proton motions coupled to electron transfer: electron transfer from $Q_A^-$ to $Q_B$ in bacterial photosynthetic reaction centers, *Biochemistry 38*, 8253−8270.
72. Ishikita, H., and Knapp, E-W. (2004) Variation of Ser-L223 hydrogen bonding with the $Q_B$ redox state in reaction centers from *Rhodobacter sphaeroides*, *J. Am. Chem. Soc. 126*, 8059−8064.
73. Xu, Q., and Gunner, M. R. (2002) Exploring the energy profile of the Q(A)(-) to Q(B) electron transfer reaction in bacterial photosynthetic reaction centers: pH dependence of the conformational gating step, *Biochemistry 41*, 2694−2701.
74. Grafton, A. K., and Wheeler, R. A. (1999) Amino acid protonation states determine binding sites of the secondary ubiquinone and its anion in the *Rhodobacter sphaeroides* photosynthetic reaction center, *J. Phys. Chem. B 103*, 5380−5387.

BI060854H